Available online at www.sciencedirect.com

ScienceDirect

Procedia Structural Integrity 24 (2019) 800–809

Structural Integrity Procedia

www.elsevier.com/locate/procedia

AIAS 2019 International Conference on Stress Analysis

Numerical investigation on the residual stresses in welded T-joints made of dissimilar materials

Alessandro De Luca[a*], Alessandro Greco[a], Paolo Mazza[b], Francesco Caputo[a]

[a]*Dept. of Engineering, University of Campania Luigi Vanvitelli, via Roma 29, Aversa, Italy*
[b] *Dept. of Chemical, Materials and Industrial Production Engineering, University of Naples Federico II, Piazzale V. Tecchio 80, Neaples, Italy*

Abstract

This study used the Finite Element (FE) method to numerically analyze the thermo-mechanical behavior and residual stresses in dissimilar welded T-joints. Residual stresses induced by the fusion arc-welding of steel joints in power generation plants are a concern to the industry. The structural integrity assessment of welded structures requires the consideration of weld-induced residual stresses for the safe operations in power plants, which may be compromised by their presence. Details on the used thermo-mechanical FE model and the results analysis are herein presented.

© 2019 The Authors. Published by Elsevier B.V.
This is an open access article under the CC BY-NC-ND license (http://creativecommons.org/licenses/by-nc-nd/4.0/)
Peer-review under responsibility of the AIAS2019 organizers

Keywords: Welding; T-Joint; Residual Stresses; Finete Element Method

1. Introduction

Thanks to the well-known benefits it offers, welding is among the most relevant joining techniques used in the structural field. Even if it is commonly used, several criticalities could compromise the efficiency of welded structures. Among these, residual stresses and distortions, which are induced by the localized heating and the subsequent non-uniform cooling (Masubuchi (1980)), play a critical role and must be avoided by designers, since they can become dangerous for the structure safety if combined with the in-service loading conditions (Citarella et al. (2016), Boccarusso et al. (2017)).

* Corresponding author. Tel.: +39-081-501-0318.
E-mail address: alessandro.deluca@unicampania.it

2452-3216 © 2019 The Authors. Published by Elsevier B.V.
This is an open access article under the CC BY-NC-ND license (http://creativecommons.org/licenses/by-nc-nd/4.0/)
Peer-review under responsibility of the AIAS2019 organizers
10.1016/j.prostr.2020.02.071

In addition, residual stresses could cause several problems during the assembly phase (Dong (2005)).

The evaluation of the residual stresses induced by fusion arc welding of steel joints is of great importance in power plants. In fact, in power plants, welded joints made of dissimilar materials are widely used to connect ferritic steel components and austenitic steel piping systems (Fellinger et al. (2018)).

Nowadays, many destructive and non-destructive techniques are available to achieve information about the stress-strain state, in terms of both amplitude and distribution, involving welded structures. However, their accuracy does not allow achieving very accurate information. In this scenario, numerical models can be very helpful for designers (Mollicone et al. (2006), Sarkani et al. (2000)).The numerical evaluation of residual stresses in dissimilar material welds is generally more challenging than that of residual stresses in similar ones because of the differences in the thermo-mechanical and metallurgical properties of the materials to be joined. Over the last two decades, there have been significant research activities using FE simulations focusing on welding residual stresses in dissimilar steel welded joints.

Akbari and Sattari-Far (2009) evaluated welding residual stresses in a dissimilar pipe joint made of A240-TP304 stainless steel and A106- B carbon steel by using 3-D finite element method (FEM). Deng et al. (2009) developed a simplification methodology to compute residual stresses in a dissimilar metal pipe joint with considering cladding, buttering, post weld heat treatment and multi-pass welding. Sepe et al. (2017) used FE model based on the "element birth and death" technique to calculate the residual stresses distribution in butt-welded joint of dissimilar material. Yaghi et al. (2013) report the FE simulation of residual stresses, due to the arc welding, of a P92 steel pipe using a nickel-based alloy (IN625) as filler material.

This paper deals with the development of a FE model for the prediction of residual stresses in welded T-joints made of dissimilar steels AISI 304 stainless, for the web, and S275JR carbon steels, for the flange. FE model is based on the "element birth and death" technique widely used in literature (Armentani et al. (2007), Armentani et al. (2012) Sepe et al. (2015)). FE model has been developed by means of ABAQUS® code. According to the performed simulations, T-joints have been made through two welding beads between web and flanges. The simulation is referred to a welding process performed by Shielded Metal Arc Welding (SMAW) technique.

Each welding bead has been made in a single pass with uniform speed and under room temperature condition. The development of this FE model is carried out in order to simplify the setup of the real welding process that authors intend to perform on such kind of joints. Moreover, it will be used for the investigation of the residual stresses that will affect the T-joints after the welding operations. In fact, at the Stat-of-the-Art, experimental methods do not allow investigating accurately on such aspect.

2. Geometry, material properties, and welding parameters

The geometry of the welded T-joint considered in this study is shown in Fig. 1. The T-joint is made of AISI 304 stainless steel plate, used for the web of the joint, welded to an S275JR carbon steel plate used for the flange. To join the two plates, two welding beads were performed, by using as filler material the S275JR carbon steel. The properties of the materials (base and filler) are taken from Boyer and Gall (1985), Holt (1996) and reported in Figs. 2 and 3. Between the two welding beads, a cooling phase, 179 s long, has been considered.

The heat input, per mm of weld length, Q, supplied by the welding machine, is defined by the following equation (1):

$$Q = (\eta \cdot V \cdot I)/v \tag{1}$$

where η is the efficiency, V is the voltage, I is the electrical current and v is the welding speed, as reported in Table 1.

The energy Q_w supplied to the welding seam during the simulation is equal to:

$$Q_w = Q \cdot L_{seam} \tag{2}$$

where: L_{seam} is the length of welding bead.

Table 1. Parameters of the welding process.

Pass	η	I [A]	V [V]	v [mm/s]	Q [J/mm]	Q_w [J]
1	0.7	85	28.5	3.0	565.25	57316.35
2				3.0	565.25	57316.35

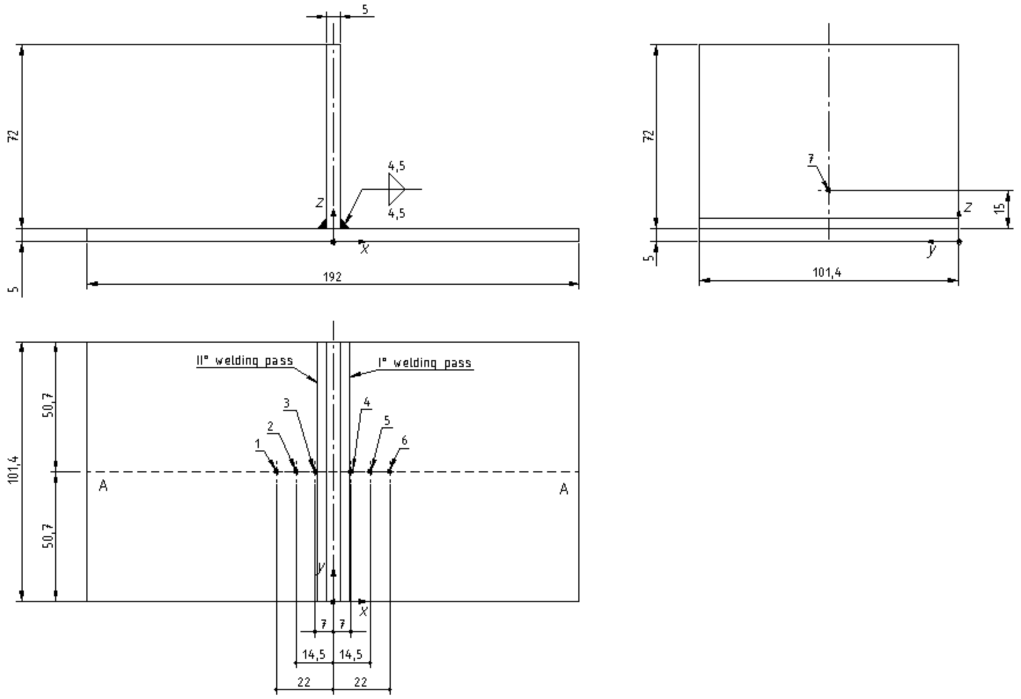

Fig. 1. Test article dimensions (in mm) and thermocouple locations.

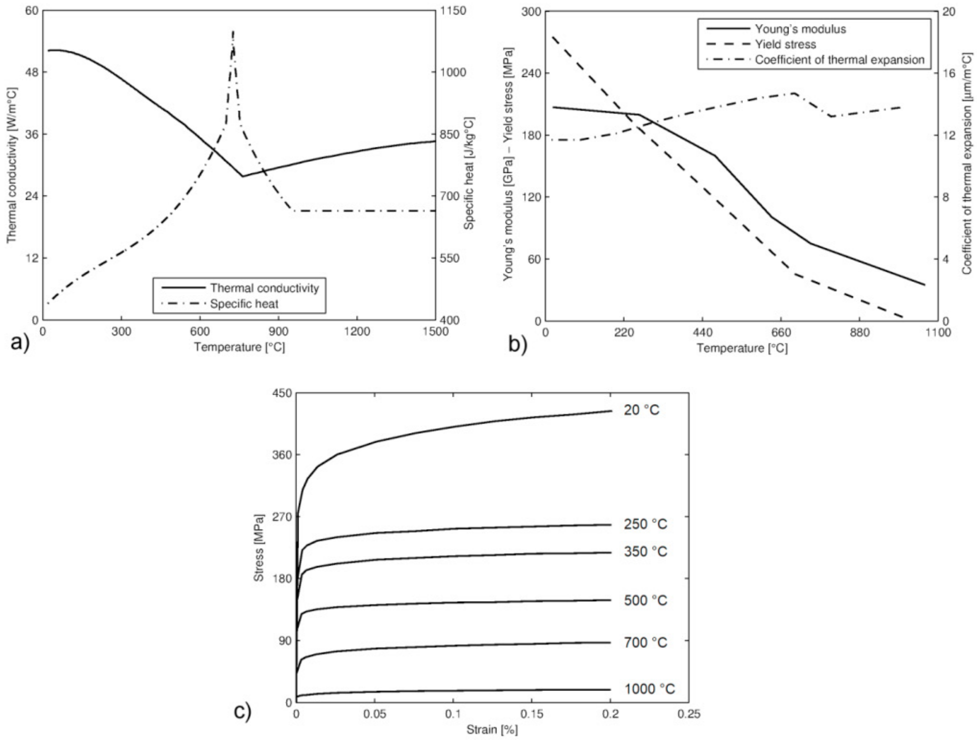

Fig. 2. S275JR steel material properties: a) thermal properties; b) mechanical properties; c) stress-strain curves at different temperatures.

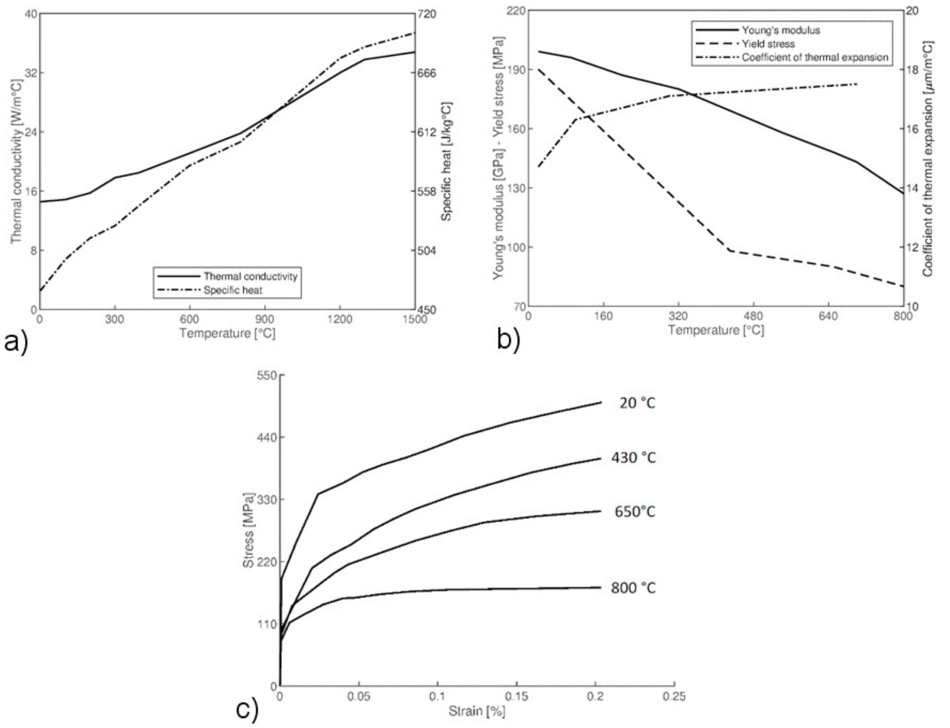

Fig. 3. AISI 304 stainless steel material properties: a) thermal properties; b) mechanical properties; c) stress-strain curves at different temperatures.

3. FE model

The uncoupled approach has been used in order to perform the thermo-mechanical simulations as well as to reduce the computational costs. Such approach consists in two consecutive analyses: the former, performed by solving independently the thermal analysis, allows achieving the temperature distribution resulting from the welding process; the latter considers the temperatures distribution, previously predicted as nodal thermal load, to evaluate the mechanical behavior. Thermal properties, shown in Fig. 2 and 3, have been implemented in the thermal analysis, while mechanical ones have been implemented in the mechanical simulation.

All analyses have been performed in ABAQUS® code, v. 6.14. FE model is based on the element birth and death technique that allows simulating the weld passes. Concerning the mesh, 8-nodes 3D finite elements have been used. Specifically, DC3D8 finite element has been used for the thermal analysis, allowing introducing the temperature as unique degree of freedom for each node, and C3D8 finite element, characterized by the three translations as degrees of freedom for each node, has been used for the mechanical analysis. FE model counts a total of 12168 finite elements and 14715 nodes. As shown in Fig. 4, a finer mesh has been developed for the chamfer region; a transition mesh for the HAZ (Heat Affected Zone) region and a coarser mesh, with a linear bias, for the other parts of the joint have been generated.

According to Fig. 4, it can be noticed that the modelling of the welded T-joint involves also the weld bead modelling. However, with reference to birth and death technique, the first analysis step is addressed to deactivate it, by multiplying finite elements stiffness that compose it by a reduction factor (i.e. 10^{-6}). In this way, it is possible to exclude it from the analysis.

The progressive reactivation of the finite elements composing the weald bead, with the main goal to simulate the added material provided during the welding process, is carried out by separating the two weld beads in 26 groups of finite elements, respectively. Subsequently, when the groups of elements need to be reactivated, in order to simulate the added material, the reduction factor previously multiplied for their properties is being progressively removed, according to the welding velocity.

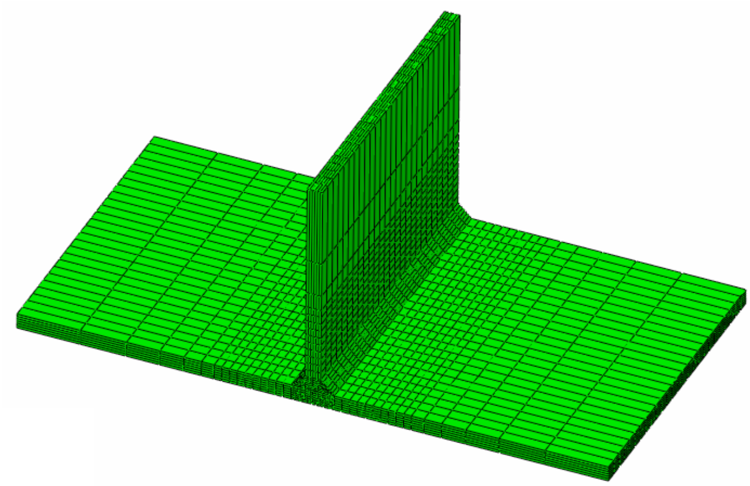

Fig. 4. FE model.

The energy Q_w (Table 1) was applied to each group of elements during the time t_{weld} (which is the time needed to cover the length of each single group) as volumetric flux.

Before starting the simulation of the second weald bead, an analysis step, 179 s long, is arranged to simulate the cooling time, which usually elapses between the two operations. Finally, a load step, 2112 s long, has been set to model the plate cooling phase up to the room temperature, of about 50 °C.

Concerning the boundary conditions, specific film conditions have been applied on T-joint free-surfaces in order to simulate the heat transfer with the environment and, in particular, the convective and radiative heat losses. For this purpose, and in order to simplify the modelling, a unique temperature dependent convective film coefficient (Fig. 5), given by the sum of the temperature dependent convective and radiative film coefficients, has been introduced in the model for characterizing the T-joint free-surfaces.

Concerning to the numerical characterization of the materials, all thermo-mechanical properties have been introduced in the FE model as a function of the temperature, as shown in Fig. 2 and 3.

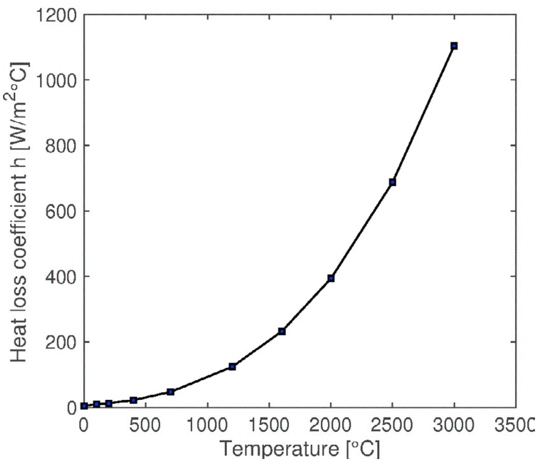

Fig. 5. Heat loss convective coefficient.

4. Results

Fig. 6.a shows the temperature distribution during the first weld pass at welding time of 16.9 s. The center of the welding arc at this time is positioned at y = 50.7 mm. It can be noticed that, in the selected frame, some elements have to be still reactivated. Fig. 6.b shows the temperature distribution involving the flange along the transverse direction (x) calculated when the welding torch passes the midsection (y = 50.7 mm) at z = 2.5 mm.

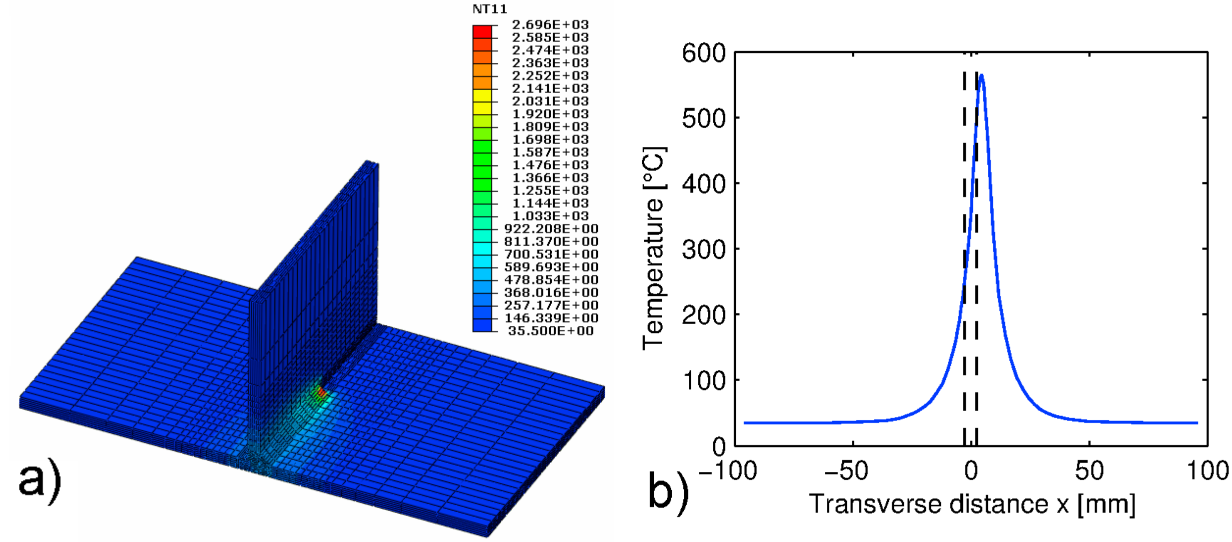

Fig. 6. a) Temperature distribution (in °C) at time t = 16.9 s in the T-joint; b) Transverse temperature distribution in the flange at midsection (y = 50.7 mm and z = 2.5 mm) during passing arc t =16.9 s.

Fig. 7.a shows the temperature distribution during the second pass, at welding time of 212.8 s. The center of the welding arc at this time is positioned at y = 50.7 mm. It can be noticed that, in the selected frame, some elements have to be still reactivated. Fig. 7.b shows the temperature distribution of the flange along the transverse direction (x) calculated when the welding torch passes the midsection (y = 50.7 mm) at z = 2.5 mm.

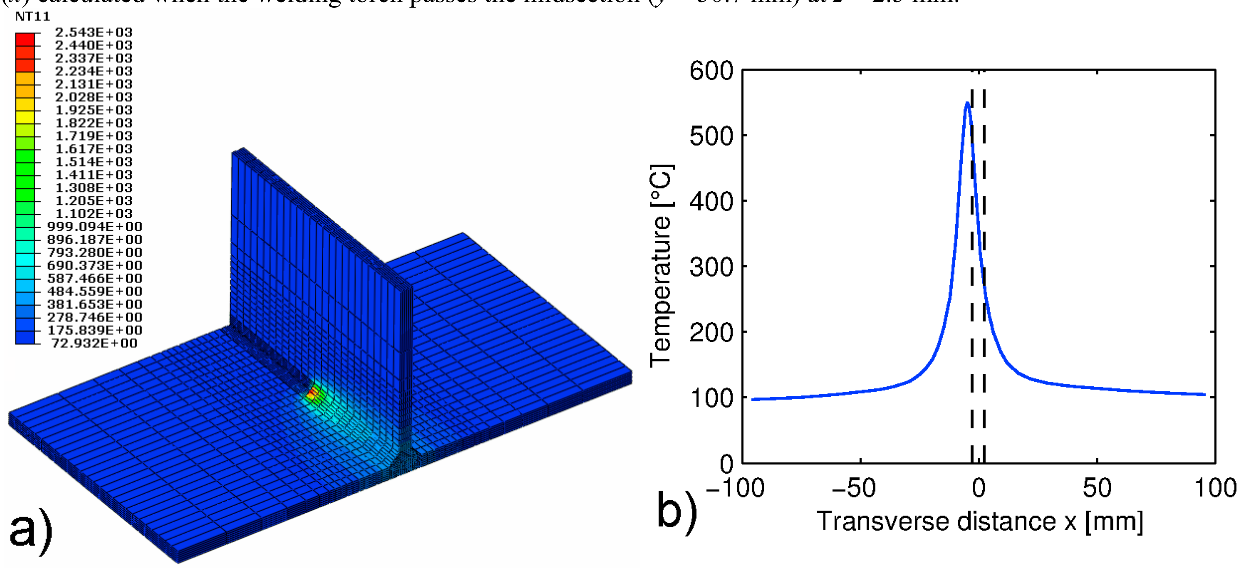

Fig. 7. a) Temperature distribution (in °C) at time t = 212.8 s in the T-joint; b) Transverse temperature distribution in the flange at midsection (y = 50.7 mm and z = 2.5 mm) during passing arc t =212.8 s.

Fig. 8 shows the temperatures histories predicted in correspondence of the seven nodes, six on the flange and one on the web, shown in Fig. 1.

From Fig. 8 it can be observed that the variations of temperature versus time have the same tendency for all seven selected locations. During the first pass, before the arrival of the welding arc (t < 16.9 s), the temperature remains close to the room one. When the welding torch approaches the cross section at y = 50.7 mm (t = 16.9 s), the temperatures of these points increase to their respective maximum at different rates. The values of temperature at points 4, 5 and 6, placed closer to welding torch, are higher than that at points 1, 2, and 3, placed on the opposite side and far from the welding torch. As the welding torch moves away from the cross section (t > 16.9 s), the temperatures at these points decrease gradually at different rates.

Similarly, during the second pass, when the welding torch approaches the cross section at y = 50.7 mm (t = 212.8 s), the temperatures at these points increase to their respective maximum at different rates. The values of temperature at points 1, 2 and 3 (placed more close to welding torch) are higher than that of the points 4, 5, and 6 (placed on the opposite side and far of welding torch). Anyway, in this case, the values of temperature at points 4, 5, and 6 are higher than that at points 1, 2 and 3 during the first pass. In fact, in correspondence of the first instant of the second pass, the temperature of plates is about T = 70 °C, which is higher than the room temperature. Although the overall tendency of these temperatures versus time curves is essentially the same, there are significant differences in the peaks, as better shown in Fig. 9, by setting the time upper limit to 500 s.

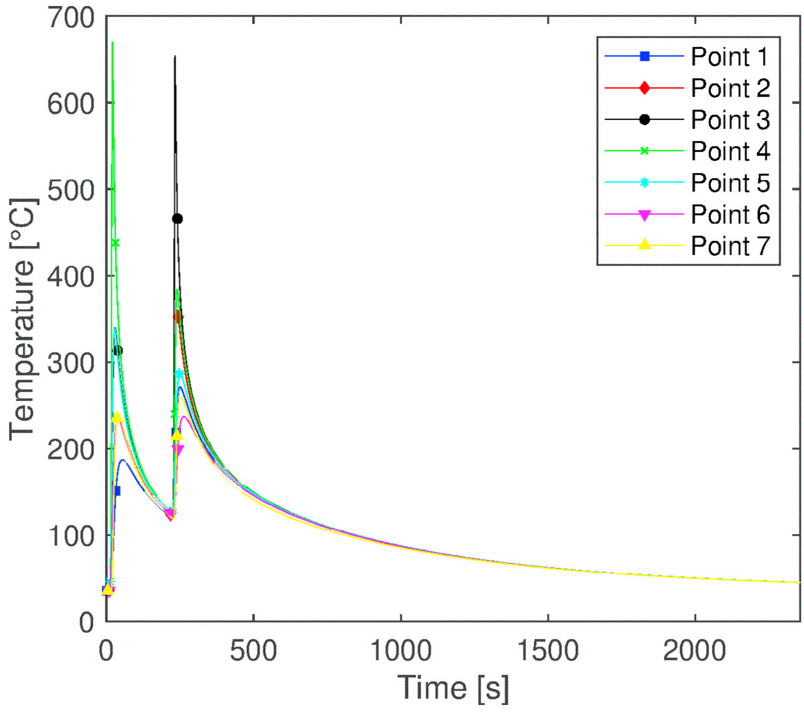

Fig. 8. Predicted temperature histories (at y = 50.7 mm) at different distances from the central line.

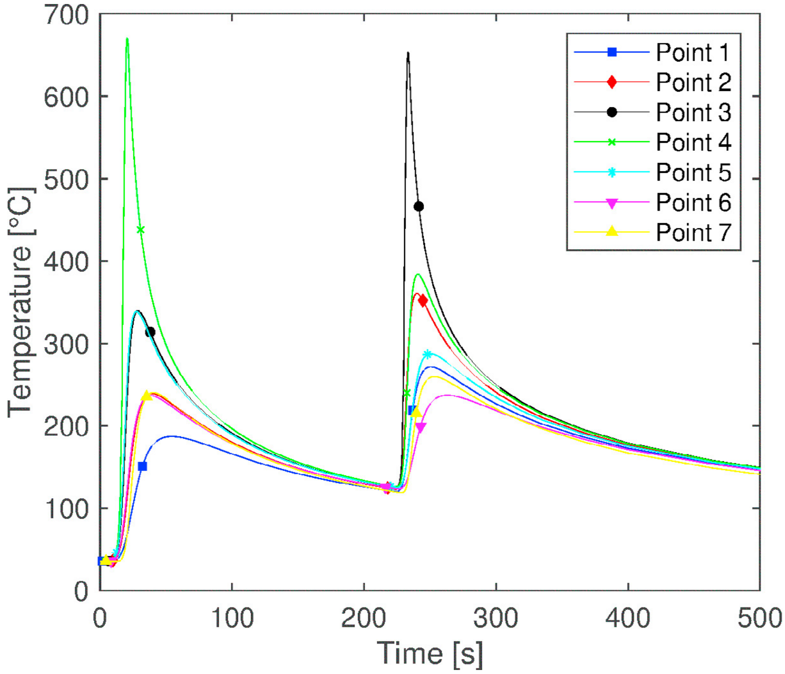

Fig. 9. Predicted temperature histories (at y = 50.7 mm) at different distances from the central line up to 550 s.

Fig. 10.a shows the transversal residual stresses distribution over the joint while Fig. 10.b shows the transversal stresses distribution along the transverse directions, x-axis, with respect to the welding bead, after the cooling phase.

Fig. 11.a shows the longitudinal residual stresses distribution over the joint, while Fig. 11.b shows the longitudinal stresses distribution along the transverse directions, x-axis, with respect to the welding bead, after the cooling phase.

It is possible to observe how the longitudinal stresses (Fig. 11) reach higher values than the transversal ones (Fig. 10) and how both distributions are quite symmetric with respect to the joint axis, with some differences due to the non-symmetric temperatures distribution, caused by the two welding operations.

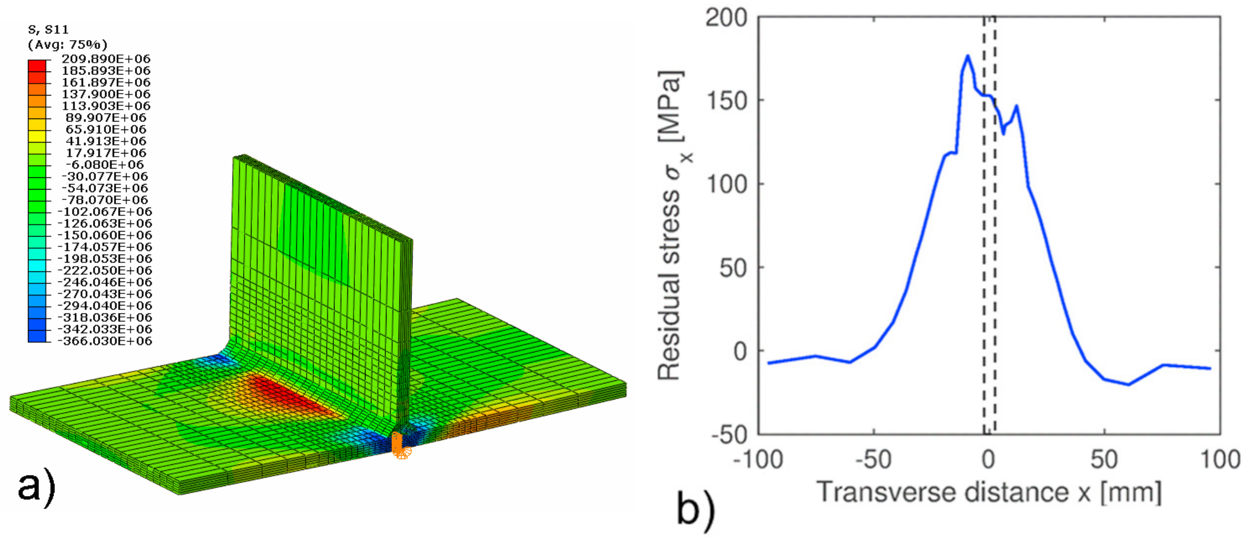

Fig. 10. a) Transversal residual stresses distribution σ_x (Pa); b) Transversal residual stresses σ_x (MPa) along the x direction at the joint midsection (y = 50.7 mm and z = 2.5 mm).

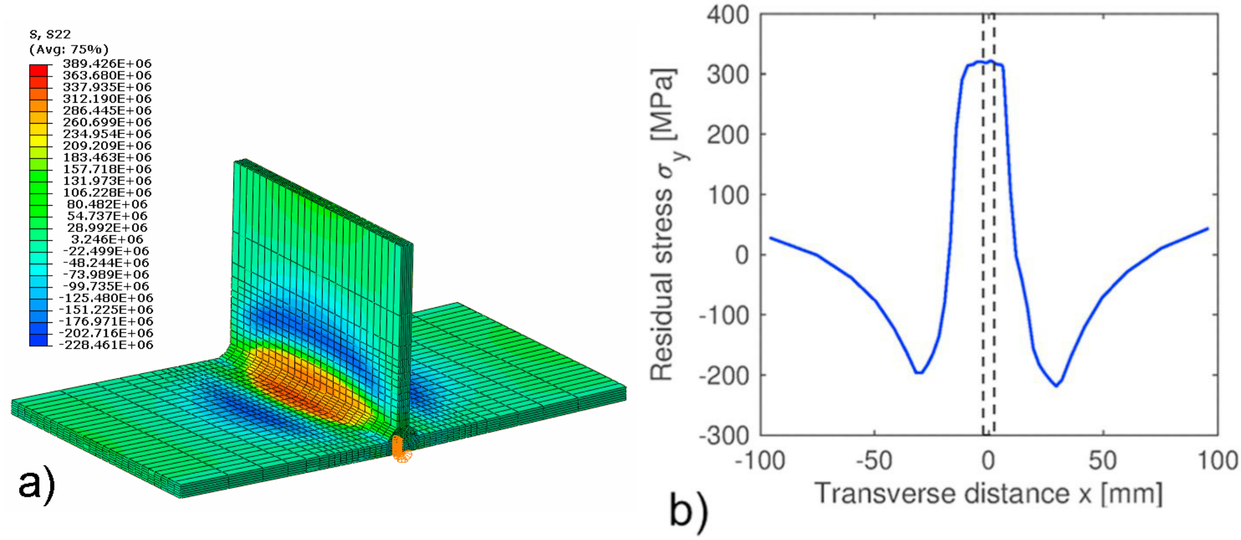

Fig. 11. a) Longitudinal residual stresses distribution σ_y (Pa); b) Longitudinal residual stresses σ_y (MPa) along the x direction at the joint midsection (y = 50.7 mm and z = 2.5 mm).

5. Conclusions

The main goal of this paper was to investigate a FE model, based on birth and death technique, for the prediction of temperature and residual stress distributions achieved during a Shielded Metal Arc Welding (SMAW) process, in a dissimilar T- joint.

Considering as input the evaluated thermal load, a subsequent mechanical analysis allowed estimating the distribution of residual stresses within the joint. The use of numerical models, able to simulate welding processes, can be useful for designers, giving accurate information about the residual stress distribution, not provided as accurately by the current experimental methods.

References

Akbari, D., Sattari-Far, I., 2009. Effect of the welding heat input on residual stresses in butt-welds of dissimilar pipe joints. International Journal of Pressure Vessels and Piping 86 (11), 769-776.

Armentani, E., Esposito, R., Sepe, R., 2007. The influence of thermal properties and preheating on residual stresses in welding. International Journal of Computational Materials Science and Surface Engineering 1 (2), 146-162.

Armentani, E., Pozzi, A., Sepe, R., 2014. Finite-element simulation of temperature fields and residual stresses in butt welded joints and comparison with experimental measurements. ASME 2014 12th Biennial Conference on Engineering Systems Design and Analysis, ESDA 2014.

Boccarusso, L., Arleo, G., Astarita, A., Bernardo, F., De Fazio, P., Durante, M., Memola Capece Minutolo, F., Sepe, R., Squillace, A., 2017. A new approach to study the influence of the weld bead morphology on the fatigue behaviour of Ti–6Al–4V laser beam-welded butt joints. International Journal of Advanced Manufacturing Technology 88 (1-4), 75-88.

Boyer, H. E. Gall, T. L., 1985. Metals Handbook. Eds., American Society for Metals, Materials Park, OH.

Citarella, R., Carlone, P., Sepe, R., Lepore, M., 2016. DBEM crack propagation in friction stir welded aluminum joints. Advances in Engineering Software 101, 50-59.

Deng, D., Ogawa, K., Kiyoshima, S., Yanagida, N., Saito, K., 2009. Prediction of residual stresses in a dissimilar metal welded pipe with considering cladding, buttering and post weld heat treatment. Computational Materials Science 47 (2), 398-408.

Dong, P., 2005. Residual stresses and distortions in welded structures: A perspective for engineering applications. Science and Technology of Welding and Joining 10 (4), 389-398.

Fellinger, J., Citarella, R., Giannella, V., Lepore, M., Sepe, R., Czerwinski, M., Herold, F., Stadler, R., the W7-X team, 2018. Overview of fatigue life assessment of baffles in Wendelstein 7-X. Fusion Engineering and Design, 136, 292-297.

Holt, J.M., 1996. Structural Alloys Handbook. Technical Ed; C. Y. Ho, Ed., CINDAS/Purdue University, West Lafayette, IN.

Masubuchi, K., 1980. Analysis of Welded Structures. Pergamon Press, Oxford UK.

Mollicone, P., Camilleri, D., Gary, T.G.F. and Comlekci, T., 2006. Simple thermo-elastic-plastic models for welding distortion simulation. Journal of Materials Processing Technology 176, 77–86.
Sarkani, S., Tritchkov, V., Michaelov, G., 2000. Efficient approach for computing residual stresses in welded joints. Finite elements in analysis and design 35 (3), 247-268.
Sepe, R., Laiso, M., De Luca, A., Caputo, F., 2017. Evaluation of residual stresses in butt welded joint of dissimilar material by FEM. Key Engineering Materials 754, 268-271.
Sepe R., Armentani E., Lamanna G., Caputo F., 2015. Evaluation by FEM of the influence of the preheating and post-heating treatments on residual stresses in welding. Key Engineering Materials 628, 93-96.
Yaghi, A.H., Hyde, T.H., Becker, A.A., Sun, W., 2013. Finite element simulation of residual stresses induced by the dissimilar welding of a P92 steel pipe with weld metal IN625. International Journal of Pressure Vessels and Piping 111-112, 173-186.